JOURNAL OF AERONAUTICAL MATERIALS
ISSN: 1005-5053
Vol. 43, Issue-01, 2023
pp. 1449-1472

MODELING AND PERFORMANCE ANALYSIS OF RECTANGULAR MINI-CHANNEL FLAT PLATE SOLAR COLLECTOR

Abhay Kumar Singh[1*], Suresh Kant Verma[2]

[1]Department of Mechanical Engineering, National Institute of Technology Patna, Patna, 80005, India
[2]Department of Mechanical Engineering, National Institute of Technology Patna, Patna, 80005, India
*Corresponding author Email Id:kumarabhay347@gmail.com
Co-author Email Id:skverma@nitp.ac.in

Abstract
In this work, mathematical models have been developed for mini-channel and conventional flat plate solar collectors(CFPSC) to analyse and compare the thermo-hydraulic performance of these collectors on the basis of various parameters like mass flow rate(MFR), water inlet temperature, and number of glazing covers. Identical dimension and similar operating conditions have been taken for both types of solar collectors. The overall model is theoretically analysed using energy equation solver. The result of this study reveals that the water outlet temperature, absorbers MPT, and overall heat loss coefficient decreases as the MFR increases. Whereas, the heat removal factor and energy efficiency increase with increase in MFR. Further it is observed that energy efficiency, useful heat gain, water outlet temperature, and heat removal factor of mini-channel flat plate solar collector (MFPSC) increases by 19.13%, 19.14%, 0.83%, and 17.63%, respectively, as compared to CFPSC for a MFR of 0.033 kg/s and at water inlet temperature of 320 K. Pressure drop and pumping power for both the collectors are almost the same for the MFR considered between 0.01 and 0.04kg/s. Furthermore, double glazing covers enhances the efficiency, heat removal factor, and useful heat gain of MFPSC by 7.0%, 1.80%, and 6.97%, respectively, over single glass cover.
Keywords: Flat plate, solar collector, heat removal factor, mini-channel, thermal performance.

1. Introduction:

Energy demand in recent decades has dramatically expanded as a result of the industrial revolution. Due to the rising demand for energy, more fossil fuels are now being consumed, which causes new environmental problems like pollution and global warming. Since fossil fuels have become so expensive in recent years, researchers are encouraged to find some alternate energy sources (Javadi, Saidur, & Kamalisarvestani, 2013). With the development of technology, the cost of producing solar thermal energy, one of the cleanest and most widely accessible sources of energy, can be reduced (Said et al., 2015). A solar collector is device which is used to transform solar radiation into thermal energy. Many different types of solar collector are available in the market, but the flat plate solar collector (FPSC) is more affordable and simpler to manufacture. The central challenges with this collector are its low outlet temperature and very low efficiency. The FPSC's performance improvement techniques can be

divided into three groups: active, passive, and hybrid. Active and hybrid methods are quite expensive and have a very sophisticated design since they need external ones aid. The efficiency and effectiveness of FPSC can be increased by passive techniques such as using phase change materials, inserts, selective coating and nano fluid as heat transfer fluid (Murugan et al., 2022). The performance of FPSC depends on the absorption of solar radiation and radiative losses. Solar selective coatings have high absorptivity for the wavelength range of 0.3–2.5 μm and low emissivity for wavelength above 2.5 μm (Wu et al., 2013). At the inner pane of the collector, double glazing with a low emitting coating was integrated to increase FPSC's efficiency. With a high absorptivity of 0.947 and a very low emissivity of 0.05 at a temperature of 80^0C, a four layer solar selective coating of CrNxOy/SiO2 was developed on a Cu(Si) substrate (Ehrmann, 2012). The electro-deposition of selective coating based on nickel/ nickel black on copper substrate have been reported by authors (Lizama-tzec, Herrera-zamora, Arés-muzio, & Gómez-espinoza, 2019) and applied on a FPSC of aperture area of 1.74 m^2 .

A new class of solid-liquid mixture known as a nanofluid has emerged as a result of advancements in nano-scale particle manufacturing technologies over the past few decades (Muhammad et al., 2016).The performance of FPSCs can be improved by using nanofluid as the heat transfer fluid. The thermo-physical characteristics of the base fluid, such as its thermal conductivity, are improved by the nanofluid produced by mixing nanoparticles with the base fluid. Due to the advancement of nanotechnology and the growing interest in enhancing the solar devices performance, a number of research has been conducted in this field (Raj & Subudhi, 2018). Kilic et al.(2018) (Kiliç, Menlik, & Sözen, 2018) investigated the experimental study using titanium dioxide-water (TiO_2/water) nanofluid in place of pure water for FPSC and observed that instantaneous efficiency of the collector increases from 36.2 % to 48.67%.The transient behaviour of a FPSC based on nanofluids (Al_2O_3/water) was investigated by Mete et al. (Mete, Akif, & Turgut, 2018) and it is found that in comparison to water, nanofluid raised the output temperature by 7.20 percent when water was substituted with TiO2-water nanofluids. It was revealed in an experimental study that the maximum efficiency improvements for FPSC for nanoparticle concentrations of 1 wt%, 3 wt%, and 5 wt% were 17.41%, 27.09%, and 33.54%.Alawi et al.(Alawi et al., 2021) observed that the energetic and exergetic efficiency of the FPSC significantly enhance when carbon-based nanofluids are used in place of metal oxides under the same operating conditions. According to Akram et al.(Akram et al., 2021), the thermal efficiency of FPSC increases by 17.45%, 13.05%, and 12.36% for functionalized graphene (f-GNPs), metal oxides ZnO, and SiO_2nanofluid, respectively, in comparison to water for same MFR of 1.6 kg/min. Farhana et al. (Farhana et al., 2021) reported that employing 0.5% Al2O3 and 0.5% crystal nano-cellulose (CNC) nanofluids, respectively, increased solar collector efficiency by up to 2.48% and 8.46%. Nabi et al.(Nabi, Pourfallah, Gholinia, & Jahanian, 2022) found that for the hybrid nanofluids SWCNT-CuO/water and MWCNT-CuO/water, respectively, at Reynolds number 10000, the heat transfer coefficient increases by 8 and 4.1% compared to Pure water. According to Mustafa et al.(Mustafa, Alqaed, & Sharifpur, 2022), thermal efficiencies of FPSC with hybrid nanofluid (aluminium oxide/copper-water) are 4.23 and 0.36% higher than those of water and (Aluminium oxide-water) mono nanofluid, respectively.

The use of inserts and twisted tape induces turbulence, which improves surface contact between

the heat transfer fluid and the FPSC hot surface, rotational flow, and better mixing of heat transfer fluid (HTF). The efficiency of FPSC can be increased by employing inserts and twisted tape, which has sparked interest in further research in this area. The usage of wire-coil inserts as a heat transfer improvement approach increased the thermal efficiency of FPSC by 4.5%, according to their numerical analysis (Pe, Garcı, & Lo, 2011). Alberto Garcia et al. (Alberto García, Martin, & Pérez-garcía, 2013) conducted an experimental analysis to examine how wire coil inserts affected the performance of FPSC and reported that their use improved thermal efficiency from 14% to 31%.For their experimental work, Sandhu et al.(Sandhu, Siddiqui, & Garcia, 2014) employed wire coil inserts, wire mesh inserts, and twisted tape, each of which had a different configuration. They showed that all three inserts raised the Nusselts number, but that concentric wire coil inserts were the most effective at low Reynolds numbers. In a comparative exploratory study, Garcia & Solano (A García & Solano, 2017) also looked at three wire coil inserts and three twisted tape inserts for FPSC. Anirudh & Dhinakaran (Anirudh & Dhinakaran, 2019) presented the numerical analysis for the investigation of the effects of thermal mixing generated by porous block inserts in the riser at various positions. The findings showed that better thermal mixing increased heat transfer. However, in these cases, the pressure drop penalty has to be paid. Vijay et al.(Vijay, Vijayakumar, Kumaresan, & Kumar, 2020) reported that incorporating twisted tape to FPSC increases efficiency from 48% to 66%.Sundar et al.(Sundar et al., 2020) revealed that when a wire coil with core-rod inserts with a p/d value of 1.79 is incorporated inside the tube, the efficiency of FPSC, using Al_2O_3/water nanofluids of concentration 0.3 wt% as heat transfer fluid, increases from 37.73 to 64.15%. A flow deviator for longitudinal flow of bi-functional rectangular inserts with a tilt angle of 30 degree were used by Vengadesan & Senthil (Vengadesan & Senthil, 2022) for their study, and they reported a maximum instantaneous efficiency of 72.93% at a MFR of 0.025 kg/s, which is 23.6% higher than that of a conventional collector. TiO2/water nanofluid with vortex generator inserts improved the thermal efficiency of FPSC with rectangular channels by 38.8%, according to Bagher et al. (Bagher, Saedodin, Hadi, Doostmohammadi, & Khaledi, 2022) .Different researchers have suggested for using the phase change material (PCM) as a way to enhance FPSC performance. Thermal energy is produced during the day, and PCMs absorb heat as a result of phase transition, releasing it at night when it is needed. The phase change material (PCM) is a cheap and efficient technique to boost solar collector performance and heat transfer (Thakur, Kumar, Kumar, & Kumar, 2021). A FPSC connected with two PCM-filled cavities was designed by Bouadila et al. (Bouadila, Fteïti, Mehdi, Guizani, & Farhat, 2014) to investigate how the weather affects solar collector performance. They revealed that 400 watts of heat may be maintained by solar collectors with an efficiency range of 25–35% for up to five hours after sunset. Al-kayiem & Lin (Al-kayiem & Lin, 2014) observed that the integration of Cu-PCM nanocomposite into the integrated thermal energy storage system increased the efficiency of FPSC by 8.4%. Mumtaz et al.(Mumtaz et al., 2018) have analysed the studies on the novel concept for integrating PCMs with FPSC. Carmona & Palacio (Carmona & Palacio, 2019) presented a thermal modelling approach for evaluating the performance of FPSC integrated with PCM. Hossain et al.(Hossain et al., 2019) fabricated a photovoltaic thermal system integrated with PCM and found that the thermal and electrical efficiency of the system was higher than that of the PV system. Badiei et al.(Badiei, Eslami, & Jafarpur, 2019)

developed the model to examine the effect of four different PCM with various melting points on the performance of FPSC. They reported that in the summer day the efficiency is increased from 33% to 46% for low melting point PCM. According to Sakhaei &Valipour (Sakhaei & Valipour, 2021), the thermal efficiency of helical corrugated tube FPSC increases from 41.5% to 48.9% when PCM is applied. Asefi et al. (Asefi, Ma, & Wang, 2022) developed the numerical model for the parametric study of the PV/thermal porous PCM system with Ag/water nanofluid as the heat transfer fluid, and they concluded that the use of porous PCM with the nanofluid increased the exergy, electrical, and thermal efficiency by 1.16%, 1.5%, and 43.1%, respectively, as compared to the PV/T-PCM system.

Sharma & Diaz (Sharma & Diaz, 2011) explored the use of mini-channels in solar collectors using numerical methods, comparing the results in terms thermo-hydraulic performance for various inlet temperatures and MFRs. A numerical model for MFPSCs has been developed by Mansour (Mansour, 2013), and the result was validated by an experimental setup of FPSC with an aperture area of 0.5 m^2, where they found that the heat removal factor (HRF) of MFPSCs was 16.1% greater than that of conventional ones. Robles et al.(Robles, Duong, Martin, Guadarrama, & Diaz, 2014) designed and developed aluminium-based MFPSC to investigate and compare its performance with copper-based CFPSC, reporting that minichannel solar collectors are 16% more efficient than conventional collectors. According to Vahidinia &Khorasanizadeh (Vahidinia & Khorasanizadeh, 2021), the thermal efficiency of large and small size minichannel FPSC is approximately the same and 13.83% and 14.22% higher than that of conventional ones, respectively, but the hydraulic performance of large MFPSC is significantly better. Different approaches have been used in the literature to enhance FPSC performance, although it should be emphasised that relatively few studies have been conducted in the area of MFPSC. Based on the previous literature reported by some researchers, it is found that the size of minichannels is small and numbers of mini-channels are high which increases the pressure drop and fabrication cost. In this study, a MFPSC of dimensions (2.8m×1.4m×0.1m) has been proposed and compared with the CFPSC of the same dimensions, on the basis of thermal and hydraulic performance. The width, height, spacing between two consecutive channels, and number of channels considered in this study, are 40mm, 2mm, 30mm and 20, respectively.

2. Methodology

The thermal performance of a CFPSC and a rectangular-shaped MFPSC under the same operating conditions and dimensions is compared by considering different parameters like water outlet temperature, absorber mean plate temperature(MPT), overall heat loss coefficient (HLC), heat removal factor (HRF), and the collector efficiency. An energy equation solver has been used to solve the mathematical model for the energy balance of a CFPSC and MFPSC. The converging absorber plate temperature is determined using an iterative method. At the converged temperature, different parameters like fluid outlet temperature, HRF, useful energy gain, and thermal efficiency have been computed.

2.1 Mathematical formulation of CFPSC

CFPSC for heating water is the most common and practical type solar collector. It is made of a sheet of metal that acts as an absorber plate, on which tubes (risers) are attached. Both sides of the tube's metal sheet act as the fin. Solar energy is collected by the metal absorber plate, where it is converted into heat and finally this energy is transferred to the water flowing inside the tube. Table 1 shows the specifications of the CFPSC and MFPSC, those which were investigated experimentally by Mansour (Mansour, 2013).

Table 1. Specification of CFPSC and MFPSC

Parameters	**CFPSC**	**MFPSC**
Area of Absorber plate (A_c)(m^2)	2	2
Length of collector(m)	2	2
Width of collector (m)	1	1
Collector Height(mm)	80	80
Diameter of Tube(mm)	10	-
Rise spacing(mm)	150	-
Thickness of absorber plate(mm)	0.5	4
Absorber plate Thermal conductivity (copper)(W/mK)	385	385
Plate Absorptivity	0.92	0.92
CoverTransmissivity	0.84	0.84
Absorber plate emissivity	0.05	0.05
Glass cover emissivity	0.85	0.85
Back insulation thickness (mm)	50	50
Side insulation thickness (mm)	25	25
Insulation thermal conductivity (copper)(W/mK)	0.025	0.025
Number of Cover	1	1
Tilt angle of Collector (degree)	45	45
Number of riser(tubes)	6	-
Number of Minichannel	-	40
Width of minichannel(mm)	-	16
Height of minichannel(mm)	-	2
Width of unit cell(mm)	-	25
Incident solar radiation on collector G_T(W/m^2)	900	900
Ambient and sky temperature(^{0}C)	20	20
Speed of wind (m/s)	7	7

Useful energy gain(UEG) for CFPSC in steady state can be expressed as (Deceased & Beckman, n.d.)

$$Q_u = A_c[S - U_L(T_{pm} - T_a)] \quad (1)$$

$$S = G_T(\tau\alpha)_e \quad (2)$$

$$(\tau\alpha)_e = 1.01\alpha_p\tau_c \quad (3)$$

$$U_L = U_t + U_b + U_e \quad (4)$$

Where, S, G_T, α_p, τ_c, U_L, U_t, U_b and U_e are known as the absorbed solar radiation, incident solar radiation per unit time per unit surface area (W/m^2), absorber plate's absorptivity, glass cover's transitivity, universal heat loss coefficient (HLC), top loss coefficient, bottom loss coefficient, and edge loss coefficient, respectively.

Convection HTC and overall HLC have been calculated using empirical relations from the literature. It is possible to calculate the top loss coefficient as (Deceased & Beckman, n.d.).

$$U_t = \left(\frac{N}{\frac{C}{T_{pm}}\left(\frac{T_{pm}-T_a}{N+f}\right)^e + \frac{1}{h_w}} \right)^{-1} + \frac{\sigma\left(T_{pm}+T_a\right)\left(T_{pm}^2+T_a^2\right)}{\frac{1}{\varepsilon_p+0.00591Nh_w} + \frac{2N+f-1+0.133\varepsilon_p}{\varepsilon_c} - N} \tag{5}$$

$$U_b = \frac{k_b}{L_b} \tag{6}$$

$$U_e = \frac{k_b}{L_e}\frac{A_e}{A_c} \tag{7}$$

Where, N, σ, T_{pm}, T_a h_w, ε_p, ε_c, L_b, L_e k_b, A_e and A_c are denoted as the number of transparent glass cover, Stefan –Boltzmann constant (5.67×10^{-8} (W/m^2K^4), the MPT in (K), the ambient temperature (in K), convection HTC for air (W/m^2K), emissivity of absorber plate, emissivity of glass cover, tilt angle of collector (degree) , thickness of back insulation (m), thickness of side insulation (m), insulation material thermal conductivity (W/mK), the side surface area and collector surface area respectively, (m^2).

Convection HTC for wind outside the cover plate has been calculated as (Deceased & Beckman, n.d.) :

$$h_w = 2.8 + 3V_w \tag{8}$$

Where, V_w is the speed of wind (m/s). The value of T_{pm} is to be assumed for the calculation of overall HLC (U_L) and it is further used to calculate the other parameter. HRF can be expressed as (Deceased & Beckman, n.d.) :

$$F_R = \frac{\dot{m}C_{pf}}{A_cU_L}\left[1-\exp\left(\frac{-A_cU_LF'}{\dot{m}C_{pf}}\right)\right] \tag{9}$$

Where F' is known as the "collector efficiency factor", can be represented as:

$$F' = \left(W\left[\frac{1}{\left(D+\left(W-D\right)F\right)} + \frac{U_L}{\pi D_i h_{fi}}\right]\right)^{-1} \tag{10}$$

Where, F is the "standard fin efficiency", can be expressed as:

$$F = \frac{\tanh\left(m(W-D)/2\right)}{m(W-D)/2} \tag{11}$$

In Eq. (11), m can be calculated as-

$$m = \sqrt{\frac{U_L}{k_p \delta_p}} \tag{12}$$

Where, δ_p is the thickness of absorber plate. The new absorber MPT can be computed from the following relation :

$$T_{pm} = T_i + \left(\frac{Q_u}{A_c U_L F_R}\right)(1-F_R) \tag{13}$$

h_{fi} is the convection HTC of the tubes fluid which is calculated for laminar flow by using following relations (Incropera & Dewitt, n.d.)

$$N_u = \frac{h_{fi} D_i}{k_f} = 3.66 + \frac{0.0668\left[(D_i / L_{tube}) R_e P_r\right]}{1+0.04\left[(D_i / L_{tube}) R_e P_r\right]^{2/3}} \tag{14}$$

$$P_r = \frac{\mu_f C_{pf}}{k_f} \tag{15}$$

$$R_e = \frac{4\dot{m}_r}{\pi D_i \mu_f} \tag{16}$$

$$\dot{m}_r = \frac{\dot{m}}{n} \tag{17}$$

Where, N_u, R_e and P_r are known as Nusselt number, Reynolds number and Prandtl number, respectively and k_f is the thermal conductivity of fluid (W/mK), μ_f is the viscosity of the fluid (kg/m-s), C_{pf} is the specific heat capacity of fluid and n is the number of tubes. These properties of the fluid are computed at the mean fluid temperature, which can be expressed as:

$$T_{fm} = T_i + \left(\frac{Q_u}{A_c U_L F_R}\right)(1-F'') \tag{18}$$

Where, F'' is the "collector flow factor" and defined as:

$$F'' = \frac{F_R}{F'} \tag{19}$$

Fluid properties can be calculated by following relations (Khanafer & Vafai, 2011)

$$\mu_f = 2.414\times10^{-5}\times10^{\frac{247.8}{T_{fm}-140}} \tag{20}$$

$$C_{pf} = -4.63\times10^{-5}\times T_{fm}^3 + 0.0552\times T_{fm}^2 - 20.86\times T_{fm} + 6719.637 \tag{21}$$

$$k_f = 0.6067\left[-1.26523 + 3.70483\left(\frac{T_{fm}}{298.15}\right) - 1.43955\left(\frac{T_{fm}}{298.15}\right)^2\right] \tag{22}$$

Water outlet temperature cab be calculated from the relation :

$$Q_u = \dot{m}C_{pf}\left(T_o - T_i\right) \tag{23}$$

Here, an iterative approach is used to solve the above non-linear equations by using energy equation solver software. In this approach, T_{pm} is initially assumed to calculate the other parameters. Further, energy balance equation has been applied, and after number of iterations the converged value of T_{pm} is obtained. The useful energy gains, HRF, absorber MPT, water outlet temperature and collector efficiency have been calculated at this final converged value of $T_{pm.}$

The collector efficiency can be computed as:

$$\eta = \frac{Q_u}{A_c G_T} \tag{24}$$

Pressure drop can be calculated as (Mahian, Kianifar, Sahin, & Wongwises, 2014)

$$\Delta P = \rho_f g(L_{tube}\sin\beta + h_L) \tag{25}$$

Where h_L is total head loss and can be expressed as :

$$h_L = \frac{8\dot{m}_r^2}{\rho_f^2 g\pi^2 D_i^4}\left(\frac{f_{Darcy}L_{tube}}{D_i} + 1.5n\right) \tag{26}$$

Where f_{Darcy}, Darcy friction factor can be defined as:

$$f_{Darcy} = 4f_{Fanning} \tag{27}$$

Where $f_{Fanning}$, Fanning friction factor can be defined as :

$$P_o = f_{Fanning}R_e \tag{28}$$

Where, P_o is Poiseuillenumber.

2.2 Mathematical formulation of MFPSC

In this study, there are twenty minichannels have been considered on the 4 mm thick absorber plate.The distance between two adjacent minichannels is assumed as a fin, and the temperature distribution between the two minichannels can be expressed using the equation below (Vahidinia & Khorasanizadeh, 2021):

$$\frac{d^2T}{dx^2} = \frac{U_L}{k\delta}\left(T - T_a - \frac{S}{U_L}\right) \tag{29}$$

The energy collection per unit length of the collector in the direction of fluid flow on both sides of the minichannel can be expressed as (Vahidinia & Khorasanizadeh, 2021)

$$\dot{q}_{Fin} = (W - a)F\left[S - U_L\left(T_b - T_a\right)\right] \tag{30}$$

Where, W, a, T_b and F are known as ,the width of the unit cell, width of the minichannel, temperature at which fluid and the absorber plate are in contact and standard fin efficiency, respectively.

The energy accumulated per unit collector length on the minichannel's surface in the fluid flow direction is defined as follows (Vahidinia & Khorasanizadeh, 2021) :

$$\dot{q}_{channel} = a\left[S - U_L\left(T_b - T_a\right)\right] \tag{31}$$

Total energy collection per unit cell per unit length of collector or useful energy gain in flow direction is (Vahidinia & Khorasanizadeh, 2021)

$$\dot{q}_u = WF'\left[S - U_L\left(T_{fi} - T_a\right)\right] \tag{32}$$

Where, F' is the minichannel collector efficiency factor:

$$F' = \left(W\left[\frac{1}{\left(a+\left(W-a\right)F\right)} + \frac{U_L}{2\left(a+b\right)h_{fi}}\right]\right)^{-1} \tag{33}$$

Where, b is the minichannel's height.

The useful energy gain that is transferred to the fluid in the minichannel can be calculated using following relation.

$$\dot{q}_u = 2(a+b)h_{fi}(T_b - T_a) \tag{34}$$

Convection HTC can be computed as follows (Vahidinia & Khorasanizadeh, 2021):

$$N_u = \frac{h_{fi}D_h}{k_f} = 4.364 + \left[0.086\left(R_eP_r\right)^{1.33}/1 + 0.1P_r\left(R_eP_r\frac{D_h}{L_{tube}}\right)^{0.83}\right] \tag{35}$$

where D_h is the minichannel's hydraulic diameter and can be represented as:

$$D_h = \frac{2ab}{a+b} \tag{36}$$

Calculating total head loss along a minichannel is as follows (Vahidinia & Khorasanizadeh, 2021)]:

$$h_L = \frac{\dot{m}_r^2}{2\rho_f^2 g a^2 b^2}\left(\frac{f_{Darcy}L_{tube}}{D_h} + 1.5n\right) \tag{37}$$

The pressure drop and pumping power for MFPSC are determined using the above expression. Pumping power for both collector can be calculated as (Vahidinia & Khorasanizadeh, 2021):

$$\text{Pumping power} = \frac{\dot{m}}{\rho_f}\Delta P \tag{38}$$

3. Model validation

The above mathematical model of nonlinear equations has been solved by an iterative method using an energy equation solver to corroborate the results reported by (Mansour, 2013) and (Vahidinia & Khorasanizadeh, 2021). Initially, data represented in table 1 was used to validate the results of the proposed model. Column 4 and column 6 in tables 2 and 3 show the percentage relative change of performance parameters for the CFPSC and MFPSC for the proposed model

in comparison to the results reported in literatures. Fig. 1 and 2 depict the variation of water outlet temperature and absorber MPT, respectively, according to MFR for CFPSC and MFPSC studied by Vahidinia & Khorasanizadeh (Vahidinia & Khorasanizadeh, 2021) and the present study. The results of this model are very similar to those found in the literature, validating the model for use in simulation work under different operating conditions.

Table 2. Comparison of output parameters for CFPSC

Parameter	**Present work**	(Mansour, 2013)	**Relative change (%)**	(Vahidinia&Khorasanizadeh, 2021)	**Relative change (%)**
$T_o(^0C)$	53.7	51.9	3.40909091	53.009	1.295111
$T_{pm}(^0C)$	63.3	63.2	0.15810277	59.98	5.38611291
F_R	0.8897	0.827	7.30471253	0.8726	1.94064575
$U_L(W/m^2K)$	4.025	4.55	-12.244898	3.968	1.42624797
η_i	0.5874	0.554	5.85246189	0.6042	2.81973817
$Q_u(W)$	1057	997.2	5.8222179	1087.5	2.84448589

Table 3. Comparison of output parameters for MFPSC

Parameter	**Present work(2)**	(Mansour, 2013)	**Relative change (%)**	(Vahidinia & Khorasanizadeh, 2021)	**Relative change (%)**
$T_o(^0C)$	55.7	54.3	2.54545455	54.3	2.54545455
$T_{pm}(^0C)$	49.6	47.3	4.74716202	47.5	4.32543769
F_R	0.971	0.958	1.34784863	0.955	1.66147456
$U_L(W/m^2K)$	3.825	3.599	6.08836207	3.81	0.39292731
η_i	0.6645	0.664	0.07527286	0.664	0.07527286
$Q_u(W)$	1196	1195	0.08364701	1195.3	0.05854556

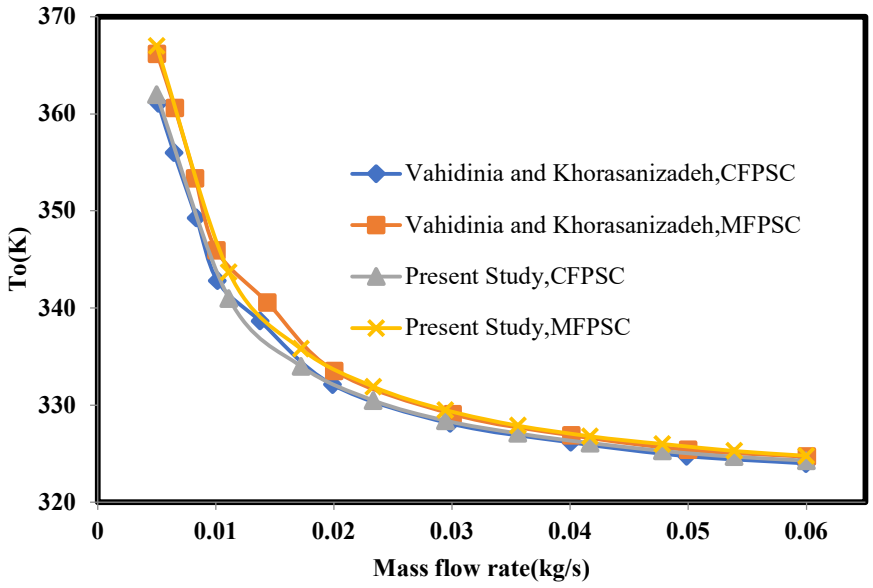

Fig.1. Compression of current study results (Water outlet temperature) with results reported by (Vahidinia & Khorasanizadeh, 2021) for CFPSC and MFPSC.

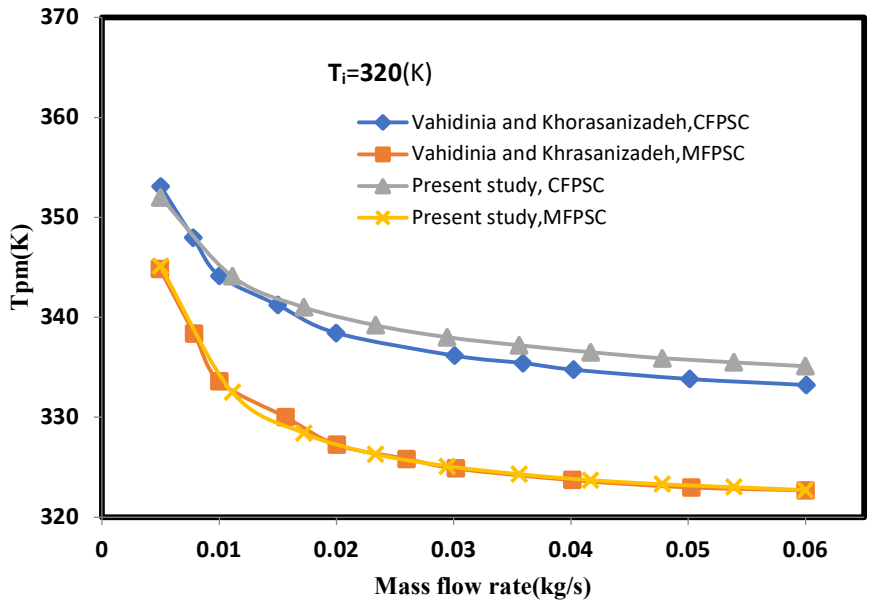

Fig.2. Compression of current study results (MPT) with results reported by (Vahidinia & Khorasanizadeh, 2021) for CFPSC and MFPSC.

4. Results and Discussions

An aluminium-based rectangular MFPSC of dimensions 2.8 m length, 1.4 m width, 100 mm height, and 20 minichannels of width 40 mm, height 2 mm, and 30 mm spacing between two minichannels have been considered as shown in Fig.3. The thickness of absorber plate is 4 mm, and the hydraulic diameter of the channel is 3.809 mm, which is about the size of a minichannel. A conventional FPSC of the same dimensions was also considered, with seven risers (tubes) of

10 mm diameter and 190 mm spacing between two consecutive risers as shown in Fig. 4. The thermo-hydraulic performance of CFPSC is compared to the aluminium-based MFPSC on the basis of water outlet temperature, useful heat gain, HRF, thermal efficiency, and pressure drop for different MFRs of water, inlet temperature, and number of glass cover. Other parameters for MFPSC and CFPSC have been listed in Table 4. Table 5 illustrates the values of different parameters for CFPSC and MFPSC at a MFR of 0.033 kg/s at steady state conditions. It is clear that all performance parameters for MFPSC except absorber MPT are higher than those for CFPSC. The water outlet temperature, HRF, useful heat gain, and energy efficiency of MFPSC increase by 0.836 %, 17.63 %, and 19.13 and 19.14%, respectively, while the absorber MPT and overall HLC decrease by 5.66 % and 6.78 %, respectively.

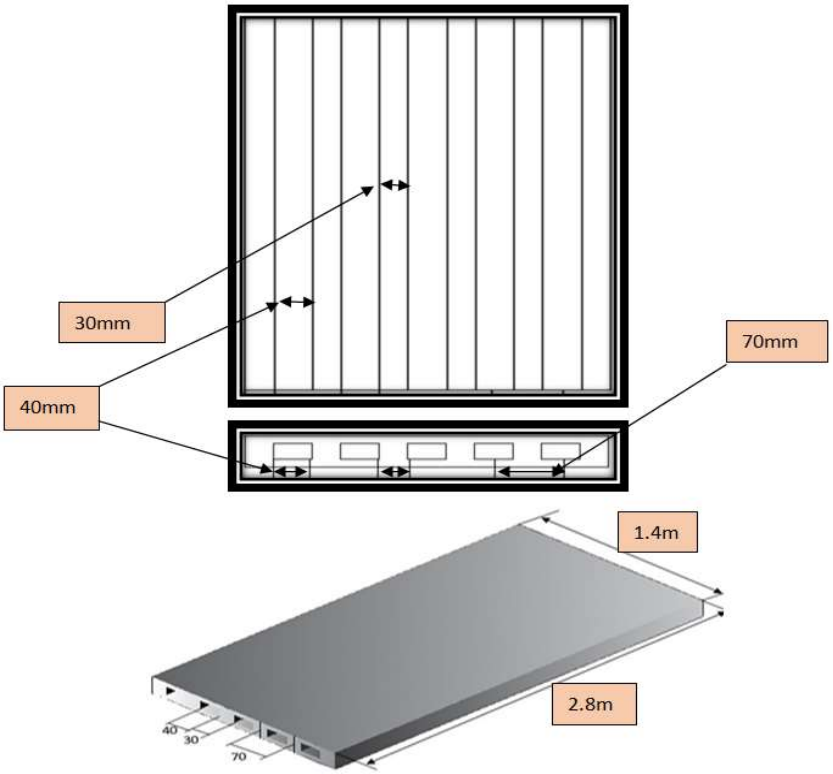

Fig.3. Schematic diagram of MFPSC with dimensions

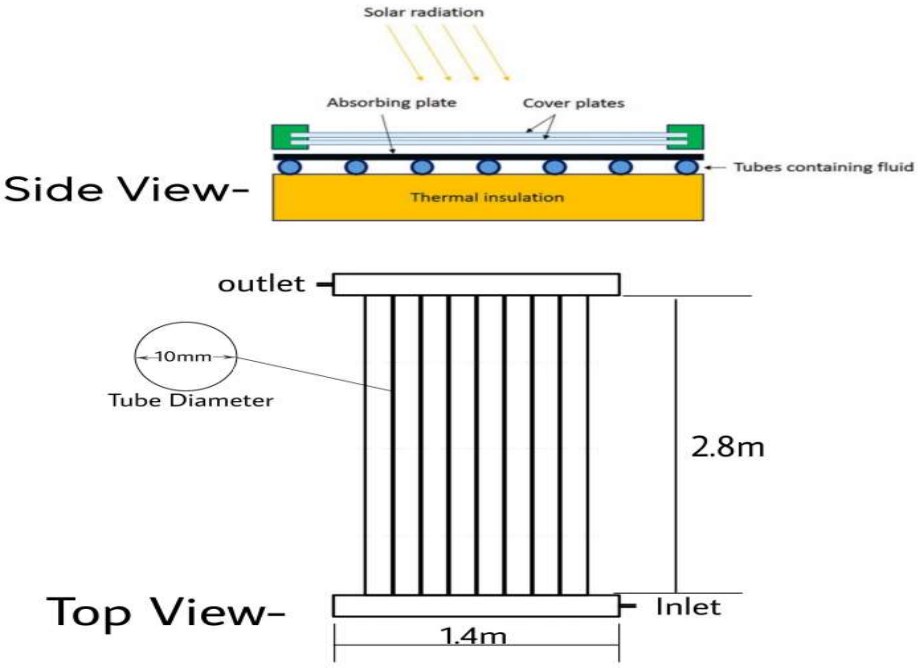

Fig.4. Schematic diagram of CFPSC with dimensions

Table 4. Specification of the proposed MFPSC and CFPSC

Parameters	**Value**
Thickness of absorber plate (mm)	0.5
Absorber plate thermal conductivity (aluminium) (W/mK)	235
Absorber plate absorptivity	0.92
Glass cover transmissivity	0.909
Absorber plate emissivity	0.09
Glass cover emissivity	0.88
Back insulation thickness (mm)	50
Side insulation Thickness (mm)	25
Insulation material thermal conductivity(W/mK)	0.025
Number of glass Cover	1
Collector tilt angle(degree)	45

Table 5 Compression of different parameters for CFPSC and MFPSC

Parameter	**(CFPSC)**	**(MFPSC)**	**Relative difference (%)**
$\mathbf{T_o(^0C)}$	334.7	337.5	0.83657
$\mathbf{T_{pm}(^0C)}$	349.6	329.3	-5.80664
$\mathbf{F_R}$	0.8013	0.9426	17.63385

U_L(W/m^{2}K)	4.316	4.014	-6.99722
η_i	0.573	0.6827	19.14485
Q_u(W)	2022	2409	19.13947

4.1. Effect of MFR on thermal performance of CFPSC and MFPSC

The performance of CFPSC and MFPSC have been compared in this section using the validated model for MFR of 0.01 kg/s to 0.07 kg/s at a constant water inlet temperature of 320 K. While laminar flow is the focus of this study, the maximum MFR is restricted to between 0.01 and 0.07 kg/s because the Reynolds number should not exceed 2300. The Reynolds numbers for CFPSC and MFPSC are 2207 and 288.7, respectively, at the maximum MFR of 0.07 kg/s.

Figure 5 and 6 depict the changes in water outlet temperature and MPT of the absorber for MFRs ranging from 0.01 kg/s to 0.07 kg/s. It is clear that the water outlet temperature for MFPSC is always higher than that of CFPSC for all MFRs between 0.01 kg/s and 0.07 kg/s at a water inlet temperature of 320 K, although it differs for MPT. The MPT for MFPSC is lower than that of CFPSC, for all MFRs were taken into consideration in this study. As seen in Fig. 5 and Fig. 6, the MPT of the CFPSC is higher than the water outlet temperature however this is not the true for the MFPSC. This is because water directly contacts the absorber plate, which causes the water to absorb more heat from the plate. As the MFR increases, the MPT and water outlet temperature for both collectors decrease. Figure 7 demonstrates how the overall HLC for both collectors decreases as the MFR increases. As the MFR rises, convective heat transfer is improved, heat transfer to the fluid increases, and the MPT decreases. For all MFRs between 0.01 kg/s and 0.07 kg/s, it is obvious from Fig. 7 that the overall HLC for MFPSC is lower than that of CFPSC. The reason is due to the lower MPT of MFPSC compared to CFPSC for considered the range of the MFR.

The effect of MFR on the collector HRF for CFPSC and MFPSC at 320K water inlet temperature is shown in Fig. 8. With a MFR between 0.01 kg/s and 0.07 kg/s, the variation in HRF for the two collectors follows a similar trend, but it is consistently larger for the MFPSC. At lower MFRs compared to higher MFRs, both collectors' HRF variance is greater. For both collectors, HRF increases as the MFR increases because the MPT decreases, minimising heat loss.

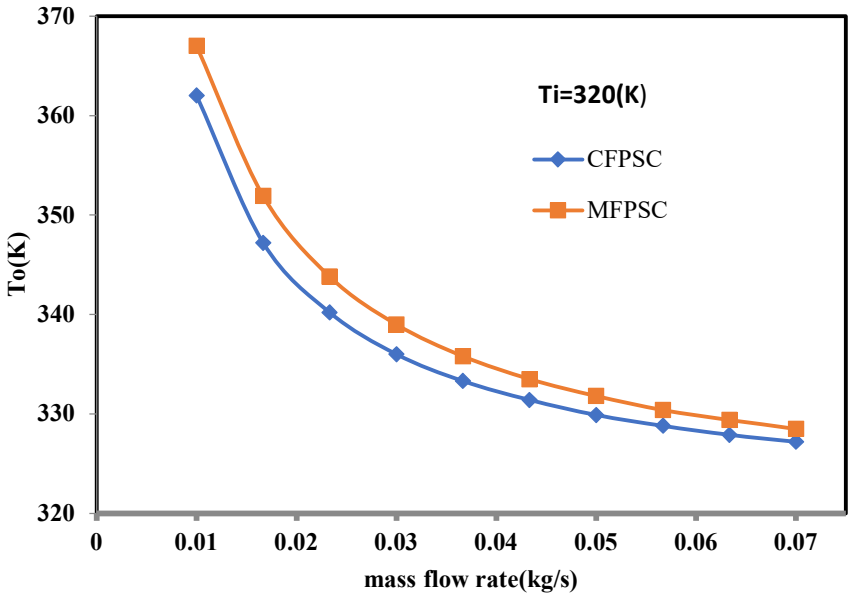

Fig.5. Variation of water outlet temperature versus MFR for CFPSC and MFPSC

Fig. 9 demonstrates the variation of energy efficiency according to MFR for the both collectors at the same water inlet temperature of 320 K. In both collectors, the variation in energy efficiency is as shown in Fig. 9 to be greater at lower MFRs than at higher MFRs. Because of the high Reynolds number at high water velocities, the collector is able to absorb more useful heat at high MFRs. The efficiency of MFPSC is higher than that of CFPSC for the same range of MFR because the absorber MPT of MFPSC is lower than that of CFPSC and, therefore, the heat losses are lower for MFPSC as compared to CFPSC.

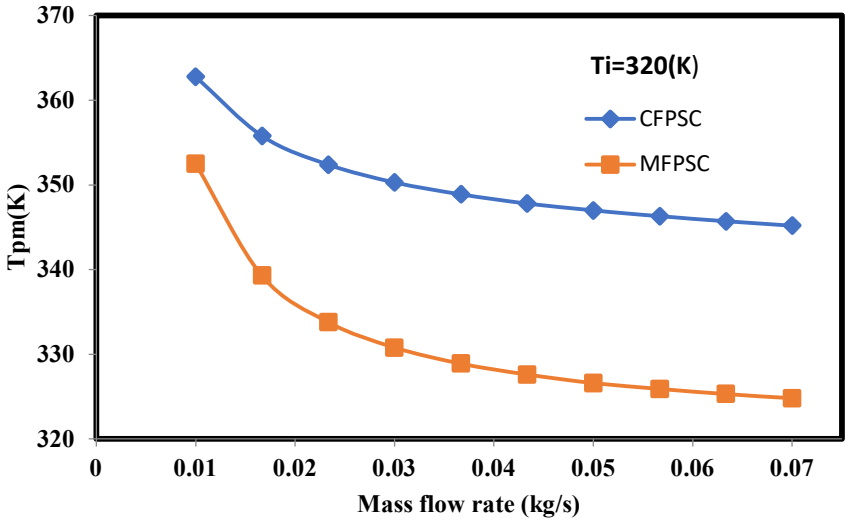

Fig.6. Variation of Absorber MPT versus MFR for CFPSC and MFPSC

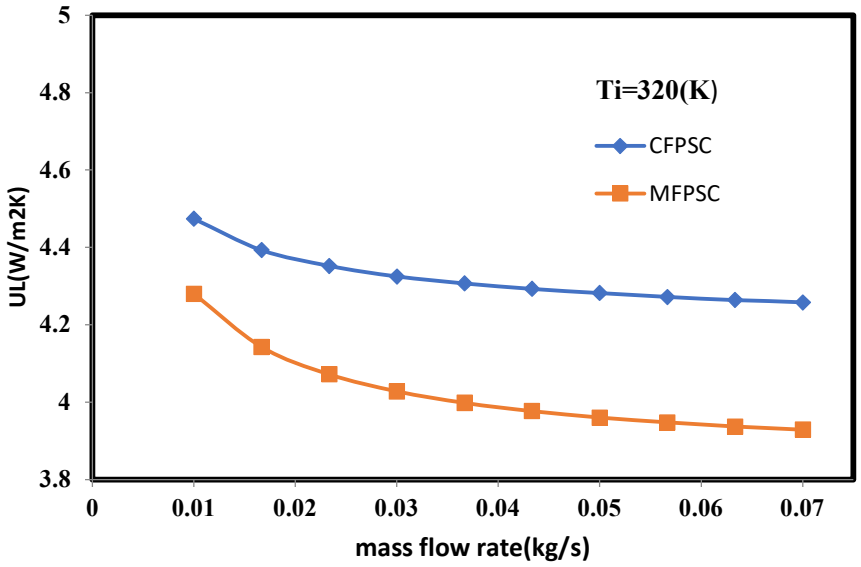

Fig.7. Variation of Overall heat loss coefficient versus MFR for CFPSC and MFPSC

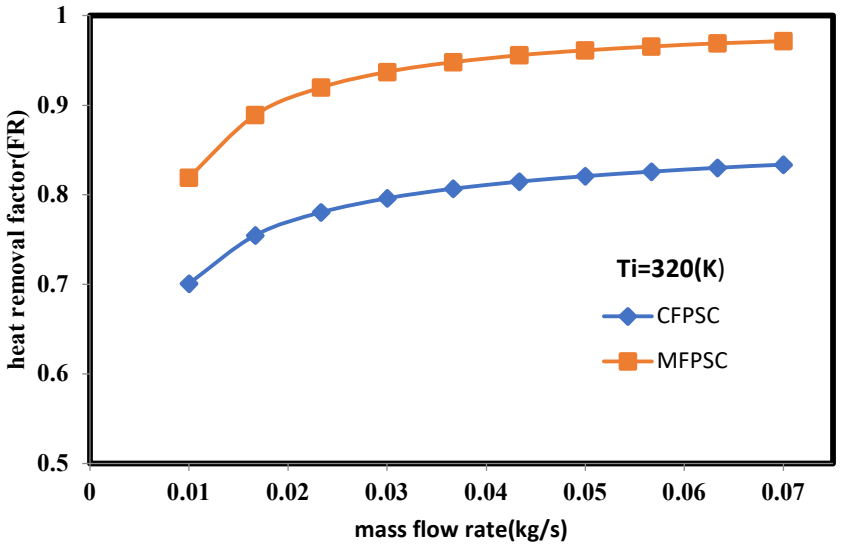

Fig.8. Variation of Heat removal factor versus MFR for CFPSC and MFPSC

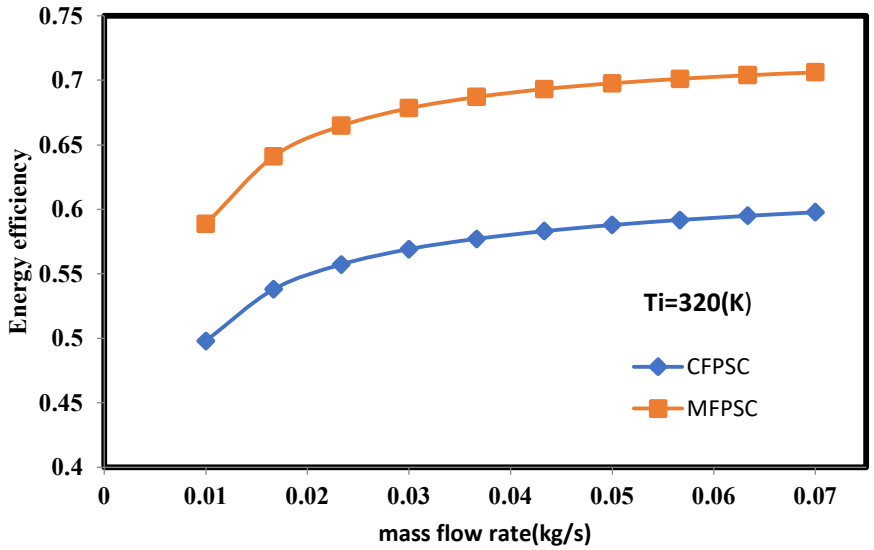

Fig.9. Variation of Energy efficiency versus MFR for CFPSC and MFPSC

4.2. Effect of MFR on hydraulic performance of CFPSC and MFPSC

The impact of MFR on pressure drop for CFPSC and MFPSC at 320K water inlet temperature is shown in Figs. 10 and Fig. 11. As it can be seen, the pressure drop for both collectors increases as the MFR increases and is nearly constant for all MFRs. Since pumping power is directly proportional to pressure drop, pumping power also increases as mass flow increases, as shown in Fig. 11. At every MFR, pumping power for both collectors is almost the same.

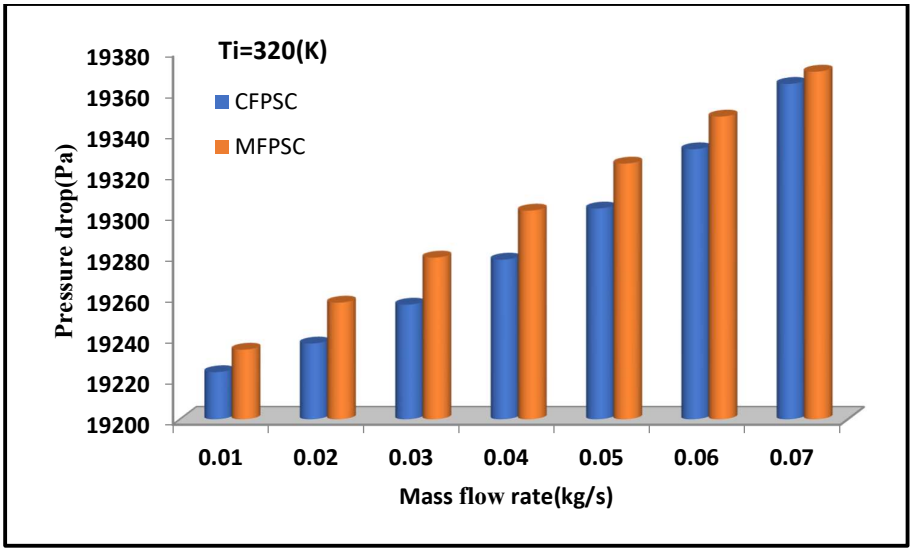

Fig.10.Effect of MFR on pressure drop for CFPSC and MFPSC.

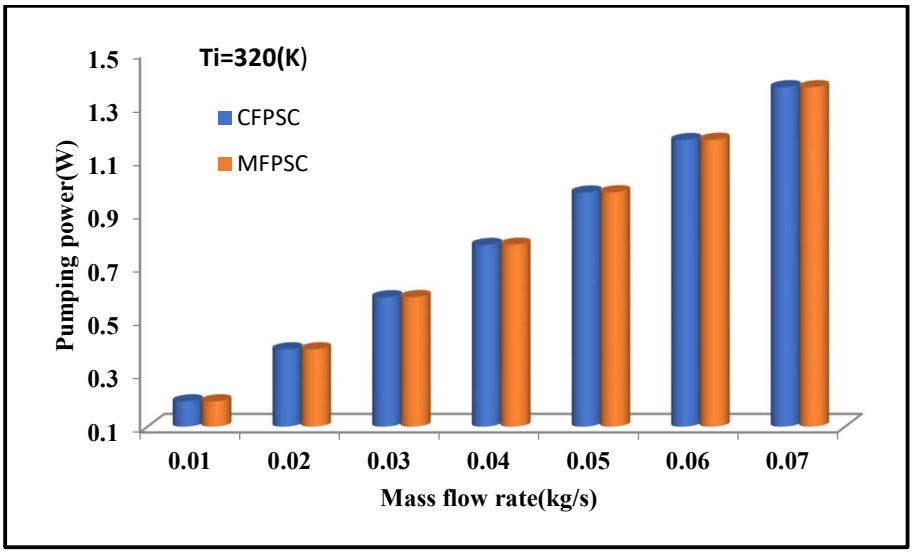

Fig.11. Effect of MFR on pumping power for CFPSC and MFPSC

4.3. Effect of water inlet temperature on thermal performance of CFPSC and MFPSC

In this section, the variation of various performance parameters with reference to the water inlet temperature for the CFPSC and MFPSC at a MFR of 0.033 kg/s has been studied. Fig. 12 demonstrates the effect of water inlet temperature on the absorber's MPT. It is obvious that as the water inlet temperature increases, the absorber MPT increases as well, and the absorber MPT of MFPSC is lower than that of CFPSC for inlet temperatures between 320 K and 350 K. Figure13 shows that HLC for both the collectors increases with increasing water inlet temperature because a higher inlet temperature results in less heat being absorbed by water, which raises the absorber MPT and increases the overall HLC. It can also be observed that HLC for MFPSC is lower that of CFPSC since water is in direct contact with absorber plate in case of MFPSC so absorption of heat is higher as compared to CFPSC. Fig. 14 shows the effect of reduced temperature on the energy efficiency of collectors at a MFR of 0.033 kg/s. The energy efficiency of both collectors' decreases as the reduced temperature rises, as seen in Fig. 14. Increased water inlet temperature causes increased reduced temperature at constant atmospheric temperature, which lowers the energy efficiency of both collectors.

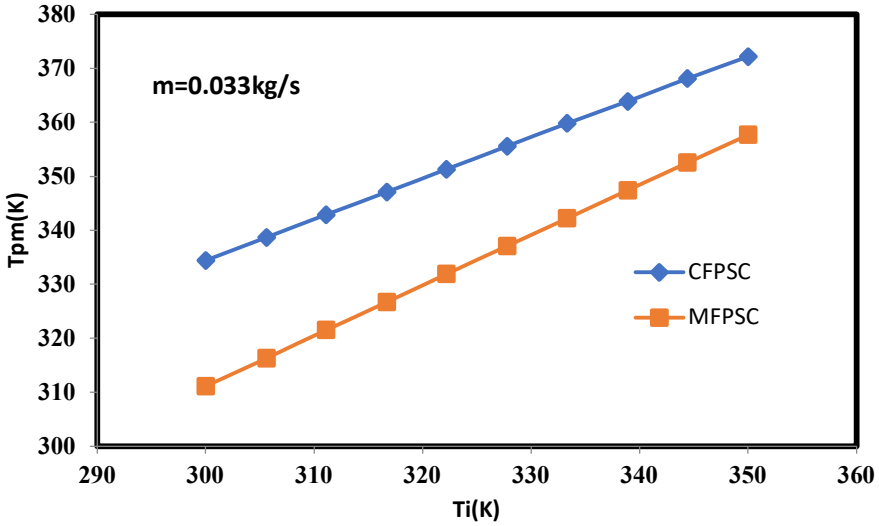

Fig.12. Effect of water inlet temperature on MPT for CFPSC and MFPSC

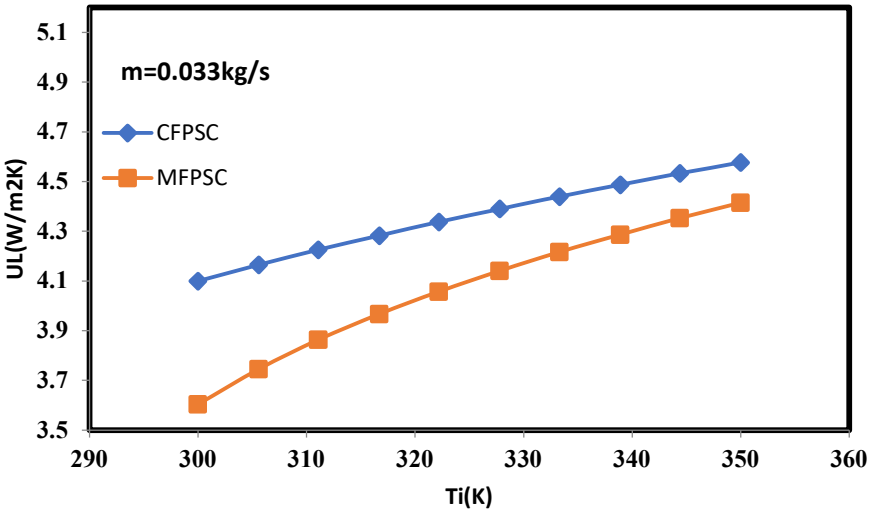

Fig.13. Effect of water inlet temperature on overall heat loss coefficient for CFPSC and MFPSC

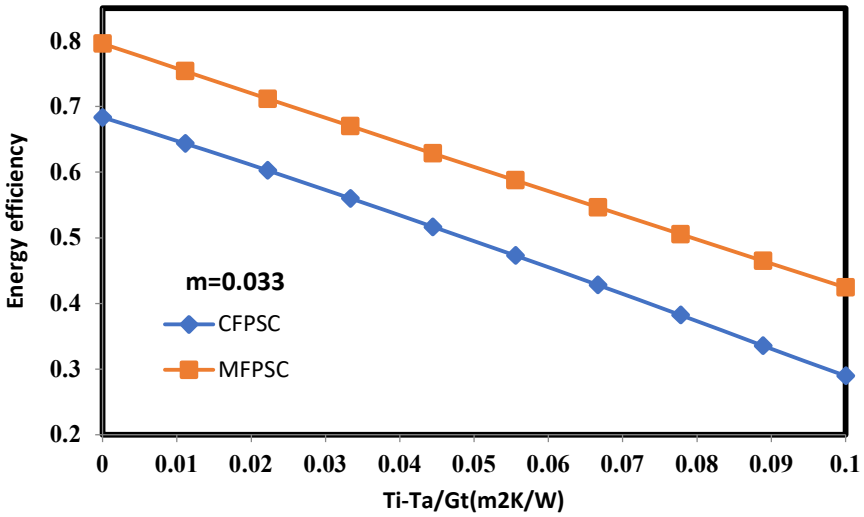

Fig.14. Effect of reduced temperature on energy efficiency for CFPSC and MFPSC

4.4. Effect of number of cover on thermal performance of CFPSC and MFPSC

At an MFR of 0.033 kg/s, Table 6 shows the effect of single and double glass covers on the different performance parameters. It is clear that using a double glass cover increases all performance parameters except absorber MPT. The top losses are the most prominent factor in all types of losses, which include convection losses and radiation losses. Increasing the number of glass covers reduces the top loss coefficient, and finally the overall loss coefficient decreases. Almost 30.61 percent of overall loss coefficients can be minimised by using double glass covers in place of single glass covers. The energy efficiency, heat removal factor, and useful heat gain increase by 7%, 1.81, and 6.97% for MFPSC, respectively.

Table 6. Effect of number of cover on performance of collectors

Parameter	Proposed MFPSC with single Cover	Proposed MFPSC with double Cover	Relative difference (%)
$T_o(^0C)$	337.5	338.7	0.355556
$T_{pm}(^0C)$	329.3	329.9	0.182205
F_R	0.9426	0.9597	1.814131
$U_L(w/m^2K)$	4.014	2.785	-30.6178
η_i	0.6827	0.7305	7.001611
$Q_u(W)$	2409	2577	6.973848

4. Conclusions

In this paper, MFPSC with dimension of 2.8 m x 1.4 m x 0.1 m is used to evaluate and analyse the thermal and hydraulic performance for various MFR and water inlet temperatures, and the

results are compared to those of a CFPSC with the same dimensions and operating conditions. The width, height, and spacing between consecutive channels are 40 mm, 2 mm, and 30 mm, respectively. A mathematical model for MFPSC has been developed, and nonlinear equations have been solved by an iterative method using an energy equation solver. By correlating the findings of the proposed work with the literature, a good agreement of the outcomes have been found and the proposed model successfully validated the results. Following are the findings of this study:

- Water outlet temperature, absorber MPT and overall HLC of MFPSC and CFPSC decreases with increase in MFR, while HRF and energy efficiency increases with increase in MFR.
- The energy efficiency, useful heat gain, water outlet temperature and HRF of MFPSC increases by 19.13 %, 19.14 %, 0.83% and 17.63%, respectively compared to CFPSC for the same geometrical operating conditions.
- The MPT and overall HLC of MFPSC decreases by 5.8% and 6.99% as compared to CFPSC.
- Pressure drop and pumping power for both the collector are almost same for the range of MFR between 0.01 and 0.07 kg/s.
- Double glass cover is preferable over a single glass cover, as the energy efficiency, heat removal factor, and useful heat gain increase by 7%, 1.81, and 6.97% respectively, for MFPSC. Further, it reduces overall HLC by 30.61% when compared to that of single glass cover MFPSC.

References

Akram, N., Montazer, E., Kazi, S. N., Elahi, M., Soudagar, M., Ahmed, W., … García, M. (2021). *Experimental investigations of the performance of a fl at-plate solar collector using carbon and metal oxides based nano fl uids*. *227*. https://doi.org/10.1016/j.energy.2021.120452

Al-kayiem, H. H., & Lin, S. C. (2014). ScienceDirect Performance evaluation of a solar water heater integrated with a PCM nanocomposite TES at various inclinations. *Solar Energy*, *109*, 82–92. https://doi.org/10.1016/j.solener.2014.08.021

Alawi, O. A., Mohamed, H., Mallah, A. R., Mohammed, H. A., Kazi, S. N., Azwadi, N., … Naja, G. (2021). *Nano fl uids for fl at plate solar collectors : Fundamentals and applications*. *291*. https://doi.org/10.1016/j.jclepro.2020.125725

Anirudh, K., & Dhinakaran, S. (2019). AC Outlet. *Renewable Energy*. https://doi.org/10.1016/j.renene.2019.06.015

Asefi, G., Ma, T., & Wang, R. (2022). Parametric investigation of photovoltaic-thermal systems integrated with porous phase change material. *Applied Thermal Engineering*, *201*(PA), 117727. https://doi.org/10.1016/j.applthermaleng.2021.117727

Badiei, Z., Eslami, M., & Jafarpur, K. (2019). Performance Improvements in Solar Flat Plate Collectors by Integrating with Phase Change Materials and Fins: A CFD Modeling. *Energy*. https://doi.org/10.1016/j.energy.2019.116719

Bagher, M., Saedodin, S., Hadi, S., Doostmohammadi, M., & Khaledi, O. (2022). The effect of vortex generator insert and TiO 2 / Water nanofluid on thermal efficiency and heat transfer

of flat plate solar collector. *Sustainable Energy Technologies and Assessments*, *53*(PC), 102617. https://doi.org/10.1016/j.seta.2022.102617

Bouadila, S., Fteïti, M., Mehdi, M., Guizani, A., & Farhat, A. (2014). Enhancement of latent heat storage in a rectangular cavity : Solar water heater case study. *Energy Conversion and Management*, *78*, 904–912. https://doi.org/10.1016/j.enconman.2013.07.094

Carmona, M., & Palacio, M. (2019). Thermal modelling of a fl at plate solar collector with latent heat storage validated with experimental data in outdoor conditions. *Solar Energy*, *177*(October 2018), 620–633. https://doi.org/10.1016/j.solener.2018.11.056

Deceased, J. A. D., & Beckman, W. A. (n.d.). *of Thermal Processes Solar Engineering*.

Edition, S. (n.d.). *No Title*.

Ehrmann, N. (2012). *Selectively coated high ef fi ciency glazing for solar-thermal fl at-plate collectors*. *520*, 4214–4218. https://doi.org/10.1016/j.tsf.2011.04.094

Farhana, K., Kadirgama, K., Mohammed, H. A., Ramasamy, D., Samykano, M., & Saidur, R. (2021). Analysis of efficiency enhancement of flat plate solar collector using crystal nano-cellulose (CNC) nanofluids. *Sustainable Energy Technologies and Assessments*, *45*(February), 101049. https://doi.org/10.1016/j.seta.2021.101049

García, A, & Solano, J. P. (2017). The role of insert devices on enhancing heat transfer in a flat-plate solar water collector. *Applied Thermal Engineering*. https://doi.org/10.1016/j.applthermaleng.2017.12.090

García, Alberto, Martin, R. H., & Pérez-garcía, J. (2013). Experimental Study of Heat Transfer Enhancement in a Flat-Plate Solar Water Collector with Wire-Coil Inserts. *Applied Thermal Engineering*. https://doi.org/10.1016/j.applthermaleng.2013.07.048

Hossain, M. S., Pandey, A. K., Selvaraj, J., Abd, N., Islam, M. M., & Tyagi, V. V. (2019). Two side serpentine fl ow based photovoltaic-thermal-phase change materials (PVT-PCM) system : Energy , exergy and economic analysis. *Renewable Energy*, *136*, 1320–1336. https://doi.org/10.1016/j.renene.2018.10.097

Javadi, F. S., Saidur, R., & Kamalisarvestani, M. (2013). Investigating performance improvement of solar collectors by using nano fl uids. *Renewable and Sustainable Energy Reviews*, *28*, 232–245. https://doi.org/10.1016/j.rser.2013.06.053

Khanafer, K., & Vafai, K. (2011). International Journal of Heat and Mass Transfer A critical synthesis of thermophysical characteristics of nanofluids. *International Journal of Heat and Mass Transfer*, *54*(19–20), 4410–4428. https://doi.org/10.1016/j.ijheatmasstransfer.2011.04.048

Kiliç, F., Menlik, T., & Sözen, A. (2018). E ff ect of titanium dioxide / water nano fl uid use on thermal performance of the fl at plate solar collector. *Solar Energy*, *164*(April 2017), 101–108. https://doi.org/10.1016/j.solener.2018.02.002

Lizama-tzec, F. I., Herrera-zamora, D. M., Arés-muzio, O., & Gómez-espinoza, V. H. (2019). Electrodeposition of selective coatings based on black nickel for flat-plate solar water heaters. *Solar Energy*, *194*(October), 302–310. https://doi.org/10.1016/j.solener.2019.10.066

Mahian, O., Kianifar, A., Sahin, A. Z., & Wongwises, S. (2014). International Journal of Heat and Mass Transfer Entropy generation during Al 2 O 3 / water nanofluid flow in a solar collector : Effects of tube roughness , nanoparticle size , and different thermophysical models. *HEAT AND MASS TRANSFER*, *78*, 64–75.

https://doi.org/10.1016/j.ijheatmasstransfer.2014.06.051
Mansour, M. K. (2013). Thermal analysis of novel minichannel-based solar fl at-plate collector. *Energy*, *60*, 333–343. https://doi.org/10.1016/j.energy.2013.08.013
Mete, A., Akif, M., & Turgut, A. (2018). Thermal performance of a nanofluid-based flat plate solar collector : A transient numerical study. *Applied Thermal Engineering*, *130*, 395–407. https://doi.org/10.1016/j.applthermaleng.2017.10.166
Muhammad, M. J., Muhammad, I. A., Azwadi, N., Sidik, C., Noor, M., & Muhammad, W. (2016). *Thermal performance enhancement of fl at-plate and evacuated tube solar collectors using nano fl uid : A review ☆*. *76*, 6–15. https://doi.org/10.1016/j.icheatmasstransfer.2016.05.009
Mumtaz, M., Khan, A., Ibrahim, N. I., Mahbubul, I. M., Saidur, R., & Al-sulaiman, F. A. (2018). *Evaluation of solar collector designs with integrated latent heat thermal energy storage : A review*. *166*(February), 334–350. https://doi.org/10.1016/j.solener.2018.03.014
Murugan, M., Saravanan, A., Elumalai, P. V, Kumar, P., Saleel, C. A., David, O., … Afzal, A. (2022). An overview on energy and exergy analysis of solar thermal collectors with passive performance enhancers. *Alexandria Engineering Journal*, *61*(10), 8123–8147. https://doi.org/10.1016/j.aej.2022.01.052
Mustafa, J., Alqaed, S., & Sharifpur, M. (2022). Evaluation of energy efficiency , visualized energy , and production of environmental pollutants of a solar flat plate collector containing hybrid nanofluid. *Sustainable Energy Technologies and Assessments*, *53*(PA), 102399. https://doi.org/10.1016/j.seta.2022.102399
Nabi, H., Pourfallah, M., Gholinia, M., & Jahanian, O. (2022). Case Studies in Thermal Engineering Increasing heat transfer in flat plate solar collectors using various forms of turbulence-inducing elements and CNTs-CuO hybrid nanofluids. *Case Studies in Thermal Engineering*, *33*(March), 101909. https://doi.org/10.1016/j.csite.2022.101909
Pe, J., Garcı, F. J., & Lo, E. (2011). *Simulation of an enhanced flat-plate solar liquid collector with wire-coil insert devices*. *85*, 455–469. https://doi.org/10.1016/j.solener.2010.12.013
Raj, P., & Subudhi, S. (2018). A review of studies using nano fl uids in fl at-plate and direct absorption solar collectors. *Renewable and Sustainable Energy Reviews*, *84*(September 2016), 54–74. https://doi.org/10.1016/j.rser.2017.10.012
Robles, A., Duong, V., Martin, A. J., Guadarrama, J. L., & Diaz, G. (2014). ScienceDirect Aluminum minichannel solar water heater performance under year-round weather conditions. *SOLAR ENERGY*, *110*, 356–364. https://doi.org/10.1016/j.solener.2014.09.031
Said, Z., Sabiha, M. A., Saidur, R., Hepbasli, A., Rahim, N. A., Mekhilef, S., & Ward, T. A. (2015). Performance enhancement of a Flat Plate Solar collector using TiO2 nanofluid and Polyethylene Glycol dispersant. *Journal of Cleaner Production*. https://doi.org/10.1016/j.jclepro.2015.01.007
Sakhaei, S. A., & Valipour, M. S. (2021). Thermal behavior of a flat plate solar collector with simultaneous use of helically heat collecting tubes and phase change materials. *Sustainable Energy Technologies and Assessments*, *46*(October 2020), 101279. https://doi.org/10.1016/j.seta.2021.101279
Sandhu, G., Siddiqui, K., & Garcia, A. (2014). International Journal of Heat and Mass Transfer

Experimental study on the combined effects of inclination angle and insert devices on the performance of a flat-plate solar collector. *HEAT AND MASS TRANSFER*, *71*, 251–263. https://doi.org/10.1016/j.ijheatmasstransfer.2013.12.004

Sharma, N., & Diaz, G. (2011). Performance model of a novel evacuated-tube solar collector based on minichannels. *Solar Energy*, *85*(5), 881–890. https://doi.org/10.1016/j.solener.2011.02.001

Sundar, L. S., Tefera, Y., Said, Z., Singh, M. K., Punnaiah, V., & Sousa, A. C. M. (2020). Energy , e ffi ciency , economic impact , and heat transfer aspects of solar fl at plate collector with Al 2 O 3 nano fl uids and wire coil with core rod inserts. *Sustainable Energy Technologies and Assessments*, *40*(June), 100772. https://doi.org/10.1016/j.seta.2020.100772

Thakur, A., Kumar, R., Kumar, S., & Kumar, P. (2021). Materials Today : Proceedings Review of developments on flat plate solar collectors for heat transfer enhancements using phase change materials and reflectors. *Materials Today: Proceedings*, *45*, 5449–5455. https://doi.org/10.1016/j.matpr.2021.02.120

Vahidinia, F., & Khorasanizadeh, H. (2021). Development of new algebraic derivations to analyze minichannel solar fl at plate collectors with small and large size minichannels and performance evaluation study. *Energy*, *228*, 120640. https://doi.org/10.1016/j.energy.2021.120640

Vengadesan, E., & Senthil, R. (2022). Experimental study on the thermal performance of a flat plate solar water collector with a bifunctional flow insert. *Sustainable Energy Technologies and Assessments*, *50*(August 2021), 101829. https://doi.org/10.1016/j.seta.2021.101829

Vijay, R., Vijayakumar, P., Kumaresan, G., & Kumar, S. G. (2020). Materials Today : Proceedings Performance study of flat plate solar collector integrated with twisted tape inserts. *Materials Today: Proceedings*, (xxxx). https://doi.org/10.1016/j.matpr.2020.04.249

Wu, L., Gao, J., Liu, Z., Liang, L., Xia, F., & Cao, H. (2013). Solar Energy Materials & Solar Cells Thermal aging characteristics of CrN x O y solar selective absorber coating for fl at plate solar thermal collector applications. *Solar Energy Materials and Solar Cells*, *114*, 186–191. https://doi.org/10.1016/j.solmat.2013.03.005